Structure and properties of $[2\text{-}NH_2C_5H_4NH][SbCl_4]$ and $[2\text{-}NH_2C_5H_4NH][SbBr_4]$

2004 J. Phys.: Condens. Matter 16 8155

(http://iopscience.iop.org/0953-8984/16/46/004)

INSTITUTE OF PHYSICS PUBLISHING JOURNAL OF PHYSICS: CONDENSED MATTER

J. Phys.: Condens. Matter **16** (2004) 8155–8172 PII: S0953-8984(04)83574-4

Structure and properties of $[2\text{-}NH_2C_5H_4NH][SbCl_4]$ and $[2\text{-}NH_2C_5H_4NH][SbBr_4]$

B Kulicka[1], R Jakubas[1], G Bator[1], Z Ciunik[1] and W Medycki[2]

[1] Faculty of Chemistry, University of Wrocław, Joliot-Curie 14, 50-383 Wrocław, Poland
[2] Institute of Molecular Physics, PAS, M Smoluchowskiego 17, 60-179 Poznań, Poland

Received 16 July 2004, in final form 20 October 2004
Published 5 November 2004
Online at stacks.iop.org/JPhysCM/16/8155
doi:10.1088/0953-8984/16/46/004

Abstract

The crystal structures of $[2\text{-}NH_2C_5H_4NH][SbCl_4]$ (2-APyHSbCl$_4$) and $[2\text{-}NH_2C_5H_4NH][SbBr_4]$ (2-APyHSbBr$_4$) are determined at 100 K. Both compounds crystallize in the monoclinic space group: $P2_1/c$. The structure is composed of SbX_4^- (X = Cl, Br) ions which form infinite chains through the crystal via halogen linkages. The structural phase transformations are detected by the differential scanning calorimetry and dilatometric techniques: at 402 K, close to continuous, and at 412 K, clearly discontinuous, in 2-APyHSbCl$_4$ and 2-APyHSbBr$_4$, respectively. Dielectric relaxation studies in the frequency range between 1 kHz and 25 MHz indicate reorientations of the 2-aminopyridinium (2-APyH) cations in both compounds in the low temperature phases. The proton NMR second moment, M_2, and spin–lattice relaxation time, T_1, for 2-APyHSbCl$_4$ and 2-APyHSbBr$_4$ measured between 78 and 430 K reveal the in-plane reorientation of the 2-APyH cations. The possible mechanism of the phase transitions in the title crystals is discussed on the basis of the results presented.

1. Introduction

In the family of halogenoantimonates (III) and halogenobismuthates (III) of the general formula $R_aM_bX_{(3b+a)}$ (where R denotes the organic cations, M denotes metal Sb(III) or Bi(III) and X denotes halogen atoms, Cl, Br, I) several ferroelectric crystals have been discovered. Most ferroelectric compounds crystallize either with the $R_3M_2X_9$ [1–6] or $R_5M_2X_{11}$ [7–10] composition. For the $R_3M_2X_9$ salts three out of six halogen atoms are terminal and the other three are bridging. The MX_6 octahedra may be connected to each other forming either infinite one-dimensional chains, two-dimensional layers or discrete bioctahedral or four-octahedral units. The salts crystallizing with the two-dimensional anionic sublattice have the tendency to exhibit ferroelectric properties. The other subclass, $R_5Bi_2X_{11}$, crystallize exclusively with discrete bioctahedral units $Bi_2X_{11}^{5-}$. It was shown that all salts with this

stoichiometry found so far possess ferroelectric properties. The origin of the ferroelectricity for both subclasses is the dynamical disorder of dipolar organic cations. Recently, there was found a ferroelectric crystal belonging to the chloroantimonate (III) salts containing in the structure the substituted pyridinium cations and polymeric anionic form, namely (4-NH_2PyH)$SbCl_4$. It revealed incommensurate modulated intermediate phases with the ferroelectric phase transition mechanism clearly of a displacive type [11]. This is in contrast to an order–disorder mechanism, which is characteristic of most ferroelectrics from the family of crystals presented.

The substituted pyridinium cations are usually bestowed significant dipole moment and electric polarizability. The incorporation of such cations into the crystal lattice is one of the ways to search for materials with attractive electric properties. Recently, Czapla *et al* reported a novel ferroelectric crystal containing substituted pyridinium cations—2-aminopyridinium—namely: (2-APyH)H_2PO_4 [12]. Its ferroelectric properties are dominated by a hydrogen bond configuration. It seems desirable to extend our studies on halogenoantimonates (III) and halogenobismuthates (III) incorporating in the structure the 2-APyH cations.

The results of studies on the synthesis and thermal properties of different 2-APyH analogues are described. In this work we present the crystal structure and results of dilatometric, differential scanning calorimetry (DSC), dielectric dispersion and proton magnetic resonance studies (^{1}H NMR) for the [2-$NH_2C_5H_4NH$][$SbCl_4$] (2-APyHSbCl_4) and [2-$NH_2C_5H_4NH$][$SbBr_4$] (2-APyHSbBr_4) salts crystallizing in the centrosymmetric space groups. The mechanism of the phase transitions in these two crystals is discussed.

2. Experimental details

DSC runs were recorded using a Perkin-Elmer DSC-7 in the temperature range 100–450 K.

The TGA measurements were performed on a Setaram SETSYS 16/18 instrument in the temperature range 300–500 K with a ramp rate 2 K min^{-1}. The scan was performed in flowing nitrogen (flow rate: 1 dm^3 h^{-1}).

The dilatometric measurements were performed using a thermomechanical analyser, Perkin-Elmer TMA-7, in the temperature range 100–430 K. The dimensions of the sample were of the order of $5 \times 3 \times 1$ mm^3.

The complex dielectric permittivity $\varepsilon^* = \varepsilon' - \mathrm{i}\varepsilon''$ was measured using HP 4285A and Agilent 4284A Precision LCR Meters in the frequency range between 1 kHz and 25 MHz and in the temperature range from 100 to 450 K. The dimensions of the sample were of the order of $5 \times 3 \times 1$ mm^3. The overall error in estimation of the real and imaginary parts of the complex dielectric permittivity value was less than 5% and 10%, respectively.

Measurements of the proton NMR second moment, M_2, were carried out over a wide range of temperature, 78–430 K, using a home-made wide-line spectrometer operating at 25 MHz. The second moment was calculated by numerical integration of the spectra and corrected for the finite modulation field.

The proton spin–lattice relaxation time T_1 was measured with a Bruker SXP 4-100 spectrometer working at the frequency of 90 MHz. The temperature of the sample was automatically stabilized by the standard Bruker liquid nitrogen system. The T_1 relaxation times were determined by using the π–τ–$\pi/2$ sequence of pulses for times shorter than 1 s and for longer times—by the saturation method. The powdered samples of 2-APyHSbCl_4 and 2-APyHSbBr_4 were degassed under pressure of 10^{-5} Torr and sealed under vacuum in glass ampoules.

X-ray measurements of crystals were performed on a Kuma KM4CCD κ-axis diffractometer with graphite-monochromated Mo Kα radiation. Both crystals were positioned at 65 mm from the KM4CCD camera. Six hundred and twelve frames were measured

at 0.75° intervals with a counting time of 15 s. The data were corrected for Lorentz and polarization effects. Analytical absorption corrections were also applied. Data collections, integration and scaling of the reflections and analytical absorption correction were carried out using the CrysAlis suite of programs [13]. The structures were solved using the heavy atom method with the SHELXS97 [14] program and refined by the full-matrix least-squares method on all F^2 data using the SHELXL97 [15] programs. Non-hydrogen atoms were refined with anisotropic thermal parameters using constraints for aromatic rings; hydrogen atoms were included from the geometry of molecules and were refined with isotropic displacement parameters for 2-APyHSbBr_4 or fixed for 2-APyHSbCl_4.

Crystallographic data for the structures reported in this paper (excluding structure factors) have been deposited with the Cambridge Crystallographic Data Centre, CCDC No 244602 and 244603. Copies of this information may be obtained free of charge from the Director, CCDC, 12 Union Road, Cambridge CB2 1EZ, UK (fax: +44-1223-336033; e-mail: deposit@ccdc.cam.ac.uk or http://www.ccdc.cam.ac.uk).

3. Results

3.1. The synthesis of 2-aminopyridinium (2-APyH) salts

The syntheses of halogenoantimonate (III) and halogenobismuthate (III) salts were carried out in aqueous solution with addition of hydrochloric (36%) or hydrobromic acid (48%) to prevent hydrolysis, with the ratio of $SbCl_3$ (Aldrich—99.999%) or $SbBr_3$ (Aldrich—99.99%) to the 2-aminopyridine (99%, Aldrich) 1:1 (the 2-aminopyridinium cations will be denoted in the text as 2-APyH). The salts obtained were twice recrystallized and characterized by an elemental analysis. The single crystals were grown from an aqueous solution at constant temperature (300 K). In the case of the 2-APyHSbBr_4 salt, high quality single crystals were grown from an acetonitrile solution.

3.2. X-ray studies

The x-ray studies for the title compounds were made at 100 K. Crystallographic data and details on the structure determinations of 2-APyHSbCl_4 and 2-APyHSbBr_4 are given in table 1. The unit cell view of 2-APyHSbCl_4 along the *c*-axis is shown in figure 1; infinite chains are formed similar to those found in numerous chloro- [16], bromo- [17] and iodo- [18] analogues containing pyridinium cations—[C_5H_5NH]SbX_4. In the unit cell of 2-APyHSbCl_4 there are found two independent 2-APyH cations. One of these cations (type N1) is characterized by the quite large displacement parameters of the C(1), C(2) and C(3) atoms, which indicate a possible libration in the plane of the pyridinium ring or statistical disorder of the C atoms. An attempt to split the positions of the cation atoms between two sites does not improve the refinement factor *R*. The 2-APyH cations are planar and form stacks between the chains. The bond distances and angles in the two crystallographically independent 2-APyH cations are in agreement with chemically expected values. The independent antimony atom lies at the centre of a distorted octahedral unit with all of the Cl–Sb–Cl bond angles within six degrees of 90° (see table 2). The Sb–Cl lengths fall into two ranges: the two longest bonds, 2.788 and 2.759 Å, are characteristic of bridging halogen atoms and the remaining ones (2.374–2.562 Å) correspond to the terminal bonds. The structure of the bromine analogue, 2-APyHSbBr_4, in general, is similar to that found for the chlorine one (see figure 2). It should be noted, however, that the *b* parameter of the unit cell for the chlorine analogue is nearly as twice that for the bromine one. In the unit cell of 2-APyHSbBr_4 there are found one independent 2-APyH cation and

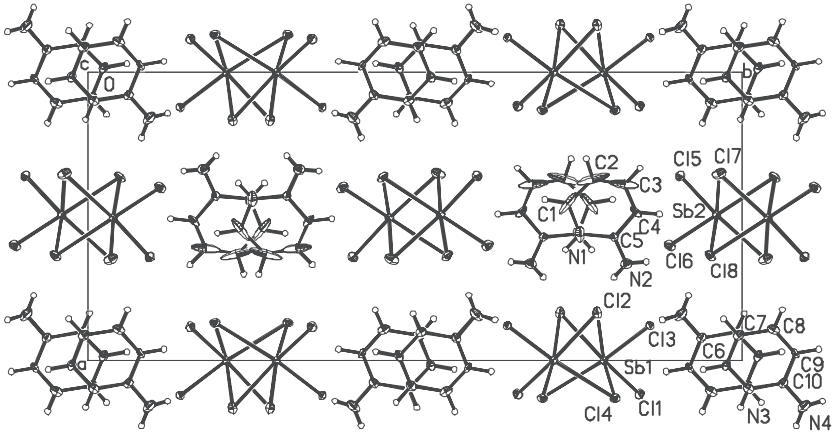

Figure 1. A unit cell view of 2-APyH-$SbCl_4$ along the *c*-axis.

Table 1. Crystal data and structure refinement.

Empirical formula	$[2\text{-}NH_2C_5H_4NH][SbBr_4]$	$[2\text{-}NH_2C_5H_4NH][SbCl_4]$
Formula weight	536.52	358.68
Temperature (K)	100(2)	100(2)
Wavelength (Å)	0.710 73	0.710 73
Crystal system	Monoclinic	Monoclinic
Space group	$P2_1/c$	$P2_1/c$
Unit cell dimensions		
a (Å)	12.4841(12)	11.3199(7)
b (Å)	13.1056(12)	25.6398(16)
c (Å)	7.4915(10)	7.5446(6)
β (deg)	105.843(10)	91.833(6)
Volume (Å^3)	1179.1(2)	2188.6(3)
Z	4	8
Calculated density (Mg m^{-3})	3.022	2.177
Absorption coefficient (mm^{-1})	15.849	3.448
$F(000)$	968	1360
Crystal size (mm)	$0.32 \times 0.28 \times 0.22$	$0.33 \times 0.30 \times 0.24$
Diffractometer	Kuma KM4CCD	Kuma KM4CCD
Theta range for data collection (deg)	3.54–28.36	3.30–28.47
Ranges of h, k, l	$-16 \rightarrow 16, -17 \rightarrow 17, -6 \rightarrow 9$	$-14 \rightarrow 14, -33 \rightarrow 33, -10 \rightarrow 7$
Reflections collected	7868	14 855
Independent reflections (R_{int})	2758 (0.0721)	0.0454
Absorption correction	Analytical	Analytical
Data/parameters	2758/138	5090/228
Goodness-of-fit (F^2)	1.023	1.175
Final $R1/wR2$ indices ($I > 2sI$)	0.0301/0.0700	0.0389/0.0891
Largest diff. peak/hole (e Å^{-3})	0.943/−1.238	1.105/−1.168

one independent Sb atom. The isotropic displacement parameters of the 2-APyH ion atoms are quite small. This means that at 100 K the cations are rather rigid in the lattice, which is in contrast to what is found in the chlorine analogue.

The cations, which occupy the spaces between polyanions, are hydrogen bonded to the chlorine or bromine atoms of the anions. The shortest N–H···Cl or N–H···Br hydrogen

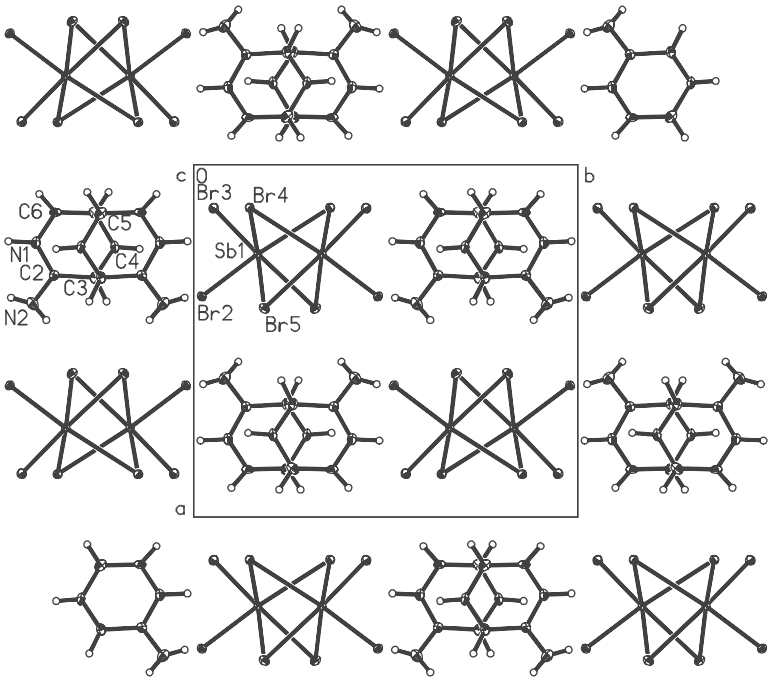

Figure 2. Crystal packing down the *c*-axis in 2-APyHSbBr_4.

Table 2. Selected bond lengths (Å) and angles (deg) in 2-APyH analogues.

[2-$NH_2C_5H_4NH$][$SbCl_4$]		[2-$NH_2C_5H_4NH$][$SbBr_4$]	
Sb(1)–Cl(3)	2.3745(13)	Sb(1)–Br(2)	2.5487(6)
Sb(1)–Cl(1)	2.4103(14)	Sb(1)–Br(3)	2.5849(6)
Sb(1)–Cl(4)	2.5279(14)	Sb(1)–Br(4)	2.7507(6)
Sb(1)–Cl(2)	2.7882(15)	Sb(1)–Br(5)	2.8811(6)
Sb(2)–Cl(5)	2.3789(14)	Br(2)–Sb(1)–Br(3)	94.84(2)
Sb(2)–Cl(6)	2.4121(14)	Br(2)–Sb(1)–Br(4)	88.918(17)
Sb(2)–Cl(7)	2.5620(15)	Br(3)–Sb(1)–Br(4)	92.104(18)
Sb(2)–Cl(8)	2.7594(15)	Br(2)–Sb(1)–Br(5)	86.649(17)
Cl(3)–Sb(1)–Cl(1)	92.90(5)	Br(3)–Sb(1)–Br(5)	91.102(18)
Cl(3)–Sb(1)–Cl(4)	88.20(5)	Br(4)–Sb(1)–Br(5)	174.734(17)
Cl(1)–Sb(1)–Cl(4)	92.45(5)		
Cl(3)–Sb(1)–Cl(2)	84.51(4)		
Cl(1)–Sb(1)–Cl(2)	88.58(5)		
Cl(4)–Sb(1)–Cl(2)	172.68(5)		
Cl(5)–Sb(2)–Cl(6)	93.18(6)		
Cl(5)–Sb(2)–Cl(7)	88.65(5)		
Cl(6)–Sb(2)–Cl(7)	91.33(6)		
Cl(5)–Sb(2)–Cl(8)	86.70(5)		
Cl(6)–Sb(2)–Cl(8)	88.37(5)		
Cl(6)–Sb(2)–Cl(8)	88.37(5)		
Cl(6)–Sb(2)–Cl(8)	88.37(5)		

contacts are listed in table 3. The nitrogen atoms of the pyridinium ring and those belonging to the NH_2 groups are involved in the hydrogen bond system. The N–H$\cdots$Cl hydrogen bonds in

Table 3. Hydrogen bonds (Å and deg).

D–H···A	d(D–H)	d(H···A)	d(D···A)	<(DHA)
		[2-$NH_2C_5H_4NH$][$SbCl_4$]		
N(2)–H(21)···Cl(2) No 1	0.78	2.62	3.378(6)	165
N(2)–H(22)···Cl(8) No 2	0.78	2.55	3.322(6)	175
N(3)–H(31)···Cl(7) No 3	0.86	2.59	3.447(5)	173
N(4)–H(41)···Cl(2) No 4	0.75	2.69	3.387(6)	154
N(4)–H(42)···Cl(6) No 4	0.87	2.65	3.346(7)	138
Symmetry transformations used to generate equivalent atoms:				
No 1 $x, -y+3/2, z-1/2$	No 2 $x, y, z-1$	No 3 $x+1, y, z$	No 4 $-x+2, -y+2, -z+1$	
		[2-$NH_2C_5H_4NH$][$SbBr_4$]		
N(1)–H(1)···Br(4) No 1	0.95(6)	2.72(6)	3.475(4)	137(4)
N(1)–H(1)···Br(3) No 2	0.95(6)	2.98(6)	3.492(4)	116(4)
N(2)–H(7)···Br(2) No 3	0.83(7)	2.95(7)	3.444(5)	121(6)
N(2)–H(8)···Br(5) No 2	0.76(9)	2.89(9)	3.570(6)	150(7)
Symmetry transformations used to generate equivalent atoms:				
No 1 $x, -y-1/2, z-1/2$	No 2 $x, -y-1/2, z+1/2$	No 3 $-x+1, y-1/2, -z+5/2$		

2-APyHSbCl$_4$ have some tendency to be linear, whereas the N–H···Br ones in 2-APyHSbBr$_4$ are strongly non-linear. One can state, however, that the hydrogen bonds in 2-APyHSbCl$_4$ and 2-APyHSbBr$_4$ systems are quite weak, which may account for the disorder of the cations at high temperatures of phase II.

3.3. Differential scanning calorimetry (DSC) and linear thermal expansion measurements

Figures 3(a), (c) show typical DSC runs on cooling and heating (with the rate of 10 K min^{-1}) for the 2-APyHSbCl$_4$ and 2-APyHSbBr$_4$ crystals. The calorimetric measurements for 2-APyHSbCl$_4$ show that we deal with at least two phases and that the phase transformation at 398/402 K on cooling/heating is reversible. The heat anomaly recorded on cooling is doubled, which probably means that in fact we deal with two closely lying phase transitions. The phase transformation II $\rightarrow$ I is associated with a relatively small entropy effect ($\Delta S =$ 3.5 J mol^{-1} K^{-1}, on heating) and is characterized by a small temperature hysteresis ($\sim$4 K) that is usually treated as evidence of a first-order phase transition. Thus we classified the phase transformation at 402 K as one of weak discontinuous type.

In the case of 2-APyHSbBr$_4$ also, only one phase transformation is detected in the temperature range 100–450 K ($T_c = 396/412$ K, on cooling/heating), which is reversible with temperature; however, the heat effects measured on cooling/heating scans are slightly different. Nevertheless, we classify the transformation as discontinuous. The relatively large entropy effect ($\Delta S = 8.4$ J mol^{-1} K^{-1}, on heating) indicates the 'order–disorder' character of this phase transformation.

Figures 3(b)–(d) present the results of the simultaneous thermogravimetric analysis and differential thermal analysis scanning for the 2-APyHSbBr$_4$ and 2-APyHSbCl$_4$ crystals. The results show that the crystals are stable up to 430 (Cl) and 450 K (Br), respectively. On the DTA curve only the anomaly at about 400 K for 2-APyHSbBr$_4$ assigned to the structural phase transition is clearly visible.

Figure 4(a) shows the results for the linear thermal expansion, $\Delta L/L_0$, obtained along the b-axis (monoclinic system, phase II) for the 2-APyHSbCl$_4$ samples. The thermal expansion was also measured along the two other crystallographic directions (a and c) and we found

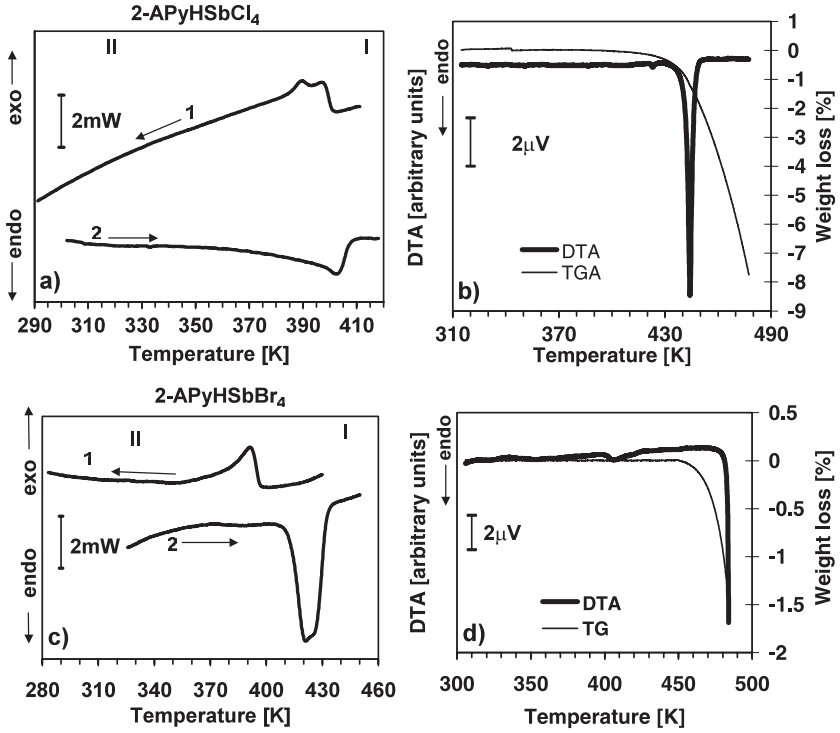

Figure 3. DSC runs on cooling and heating and simultaneous thermogravimetric analysis and differential thermal analysis scanning for the 2-APyHSbCl$_4$ and for 2-APyHSbBr$_4$ crystals (DSC with the ramp rate of 20 K min^{-1}; sample masses: 2-APyHSbCl$_4$—30.856 mg, 2-APyHSbBr$_4$—33.458 mg).

that the character of these $\Delta L/L_0$ runs was very similar to that observed along the b-axis; that is why they are not presented. We can state that dilatometric results agree well with the data obtained in the DSC measurements. The transformation at 402 K, on heating, in 2-APyHSbCl$_4$ (figure 4(a)) is accompanied by the $\Delta L/L_0$ change characteristic for mixed continuous–discontinuous transformations. This means that only a change in the value of the linear thermal expansion coefficient, $\bar{\alpha} = \Delta L/(L_0 \Delta T)$, is observed at the phase transformation temperature and no discontinuous stepwise change in $\Delta L/L_0$ is observed in the vicinity of 402 K.

In a case of 2-APyHSbBr$_4$ the dilatometric measurements were performed along a-, b- and c-axes (figure 4(b)). Along all directions the values of the thermal expansion coefficient, $\bar{\alpha}$, in the low temperature phase are positive ($\sim$6–8 $\times$ 10^{-5} K^{-1}). It should be noted that 2-APyHSbBr$_4$ shows very small anisotropy in phase II as regards to the dilatometric properties. The phase transformation at 412 K is accompanied by a rapid increase of the dimensions of the crystals; such a linear thermal expansion response is typical for phase transitions close to the discontinuous one. The $\bar{\alpha}$ values in the high temperature phase are negative along a- and b-axes and positive along the c-axis, indicating that the high temperature phase (I) reveals different dilatometric characteristics to phase II and that we are certainly dealing with a structural phase transition.

On cooling, the dilatometric anomalies are not perfectly reversible, because the compound is heated to about 15–20 K above the phase transition temperature and the crystals become unstable at their surfaces (when exposed to the air).

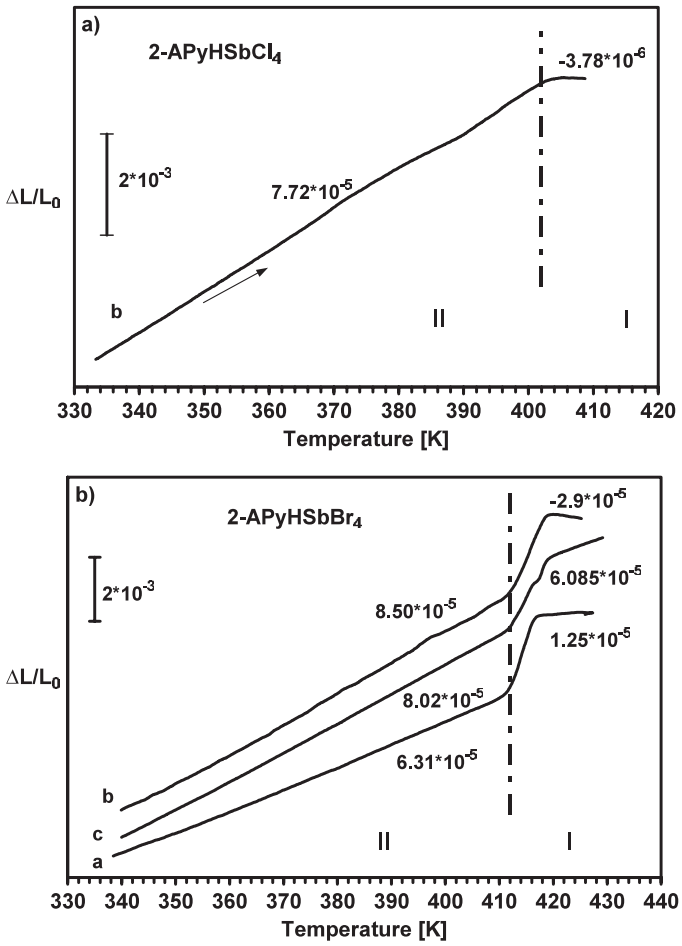

Figure 4. (a) The temperature dependence of the linear thermal expansion, $\Delta L/L_0$, measured along the *b*-axis (monoclinic system, phase II, 100 K) at a ramp rate 3 K min^{-1} for the 2-APyHSbCl$_4$ samples. (b) The temperature dependence of the linear thermal expansion, $\Delta L/L_0$, measured along the *a*-, *b*-and *c*-axes (monoclinic system, phase II, 100 K) at a ramp rate 3 K min^{-1} for 2-APyHSbBr$_4$ samples.

3.4. Dielectric relaxation studies

3.4.1. 2-APyHSbCl$_4$ salt. For 2-APyHSbCl$_4$ we performed measurements of the complex dielectric permittivity, ε^*, as a function of temperature and frequency. The purpose of these measurements was to determine the nature of the phase transition and to find the parameters of the presumed dielectric relaxation process. The temperature dependence of the real part of the electric permittivity along the *b*-axis (monoclinic system, phase II) for five selected frequencies is presented in figure 5. Over phase II, monotonic increase of ε'_b is observed and additionally a clear dispersion of ε'_b is detected. Above the II $\rightarrow$ I transformation the discrepancies between permittivity runs at different frequencies are caused most probably by the appearance of electric conductivity, which is usually observed in halogenoantimonates (III) or halogenobismuthates (III) at high temperatures. Since in phase II a clear dispersion of the real part of the dielectric permittivity has been observed, we decided to perform a detailed study of the dielectric relaxation process.

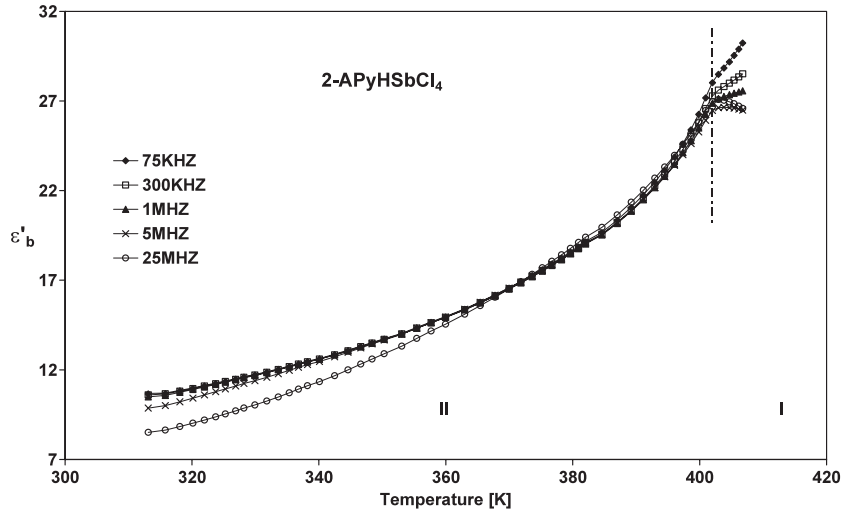

Figure 5. The temperature dependence of the electric permittivity along the *b*-axis for the 2-APyHSbCl$_4$ crystal (monoclinic system, phase II) for five selected frequencies.

Figure 6 shows the temperature dependence for the real and imaginary parts of the complex dielectric permittivity, $\varepsilon_b^* = \varepsilon_b' - \mathrm{i}\varepsilon_b''$, over phase II in the frequency range 75 kHz–5 MHz for 2-APyHSbCl$_4$ samples. The dispersion in ε_b' is accompanied by the absorption curves, the maxima of which are shifted towards higher temperatures on increasing frequency.

The Cole–Cole diagrams at selected temperatures are presented in figure 7. It was found that the dielectric response in 2-APyHSbCl$_4$ crystals is well described by the Cole–Cole relation [19]:

$$\varepsilon^* = \varepsilon_\infty + \frac{\varepsilon_0 - \varepsilon_\infty}{1 + (\mathrm{i}\omega\tau)^{1-\alpha}}, \tag{1}$$

where ε_0 and ε_∞ are the low and high frequency limits of the electric permittivity, respectively, ω is the angular frequency, τ is the mean relaxation time and α is the parameter of distribution of the relaxation times.

We have fitted the experimental Cole–Cole plots at several temperatures using equation (1) in order to estimate the relaxation parameters: ε_0, ε_∞, α and τ. The parameters of the relaxation process are collected in table 4. An important increase in the mean relaxation time τ (about one order of magnitude in the interval of 30 K) indicates a substantial slowing down of the relaxation process on cooling. The simultaneous increase in the distribution parameter value α up to about 0.45 at 265 K shows that the dielectric spectrum becomes extremely diffuse on lowering temperature. It should be noted that the value of ε_∞ ($\sim$6.1) is almost temperature independent.

The energy barrier, E_a, for the dipolar reorientation was estimated from an Arrhenius-type relationship for the macroscopic relaxation time:

$$\tau_\mathrm{macr} = C \exp\left(\frac{E_\mathrm{a}}{kT}\right). \tag{2}$$

The activation energy estimated for this process (see figure 11) is equal to 43.84 kJ mol^{-1} and is rather high for crystals of this type [20, 21].

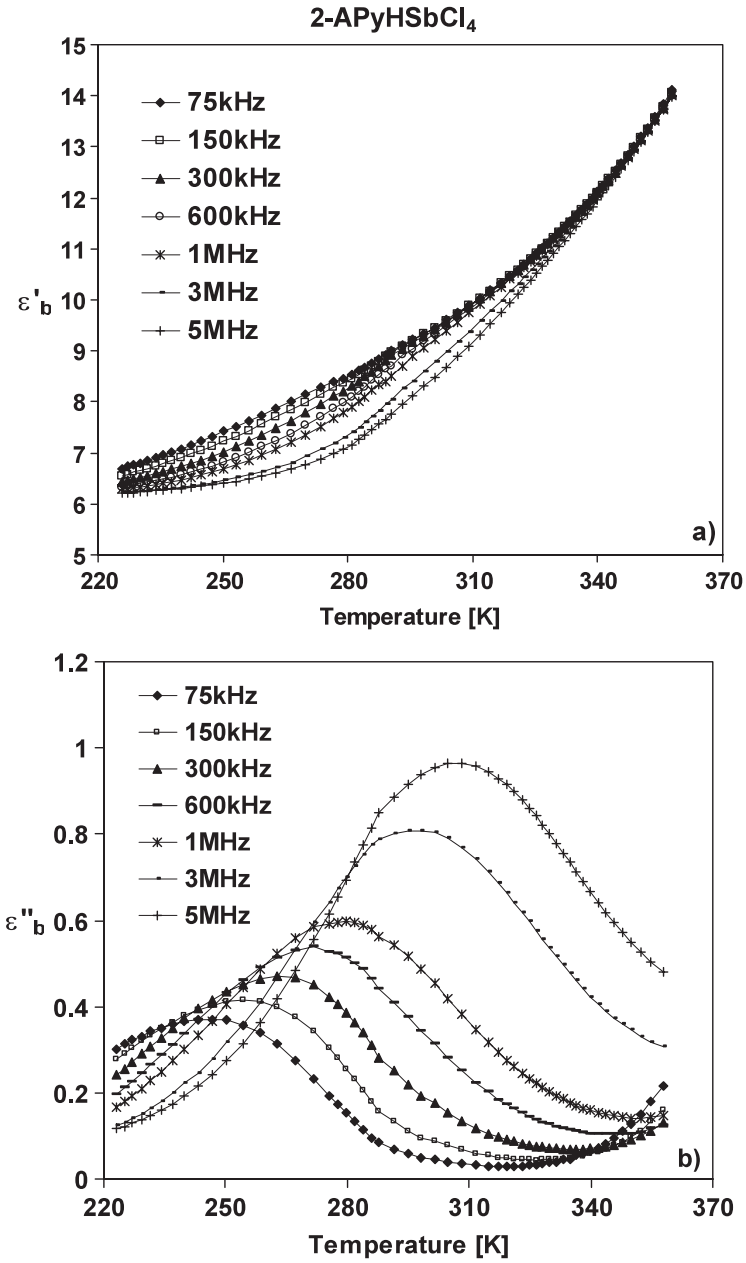

Figure 6. The temperature dependence of (a) the real and (b) the imaginary part of the complex electric permittivity, $\varepsilon_b^* = \varepsilon_b' - \mathrm{i}\varepsilon_b''$, for the 2-APyHSbCl$_4$ samples.

3.4.2. 2-APyHSbBr$_4$. The results of dielectric measurements on 2-APyHSbBr$_4$ crystals performed along the *b*-axis are presented in figure 8. The real part of the complex dielectric permittivity versus temperature curve, $\varepsilon'(T)$, exhibits an anomaly at a temperature corresponding to the phase transformation found at 412 K. The stepwise change of ε' by about five units at T_c may be connected with a releasing (on heating) of some kind of dipolar

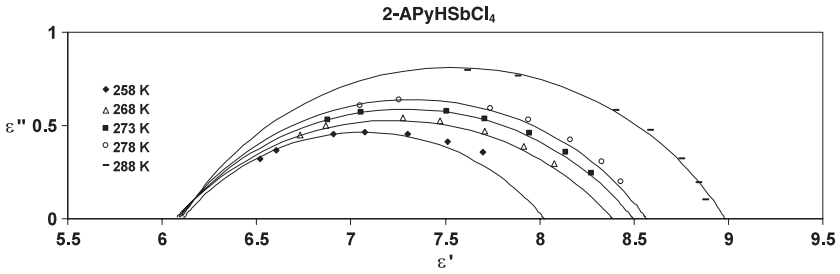

Figure 7. The Cole–Cole diagrams at the selected temperatures for phase II of 2-APyHSbCl$_4$.

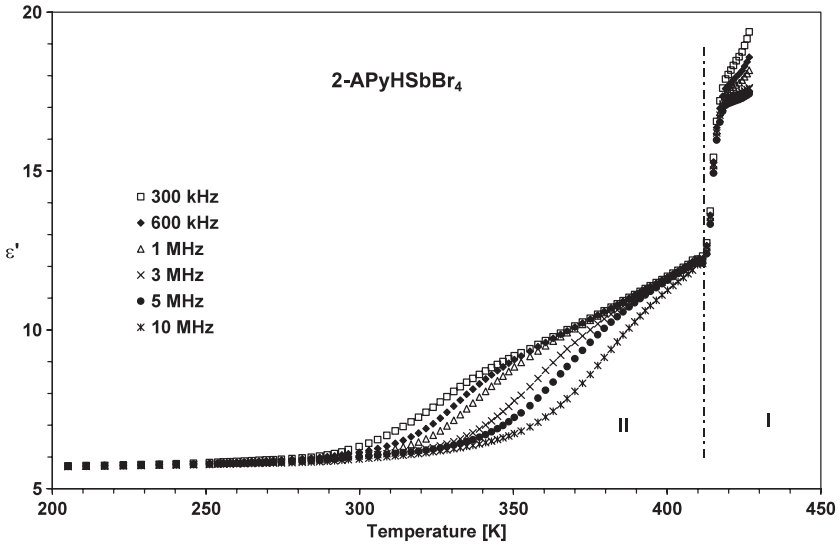

Figure 8. The temperature dependence of the electric permittivity along the *b*-axis of 2-APyHSbBr$_4$ (monoclinic system, phase II) for six selected frequencies.

Table 4. The dielectric relaxation parameters for 2-APyHSbCl$_4$ and 2-APyHSbBr$_4$.

	T (K)	τ	ε_0	ε_∞	α
2-APyHSbCl$_4$	255	1.50×10^{-4}	8.03	6.11	0.43
	265	6.17×10^{-6}	8.39	6.07	0.46
	270	1.04×10^{-6}	8.50	6.08	0.42
	275	1.52×10^{-7}	8.57	6.09	0.39
	285	4.29×10^{-8}	8.98	6.10	0.35
2-APyHSbBr$_4$	244	2.50×10^{-7}	6.98	5.79	0.14
	284	1.30×10^{-7}	7.48	5.96	0.10
	304	8.90×10^{-8}	7.77	6.02	0.12
	334	5.85×10^{-8}	8.50	6.27	0.07
	354	2.90×10^{-8}	9.41	6.33	0.08
	374	2.50×10^{-7}	10.36	6.33	0.07

reorientation above this temperature. The reorientations may be related to the motions of the parts of the 2-APyH cations or their motion as a whole. The cationic motion is surely

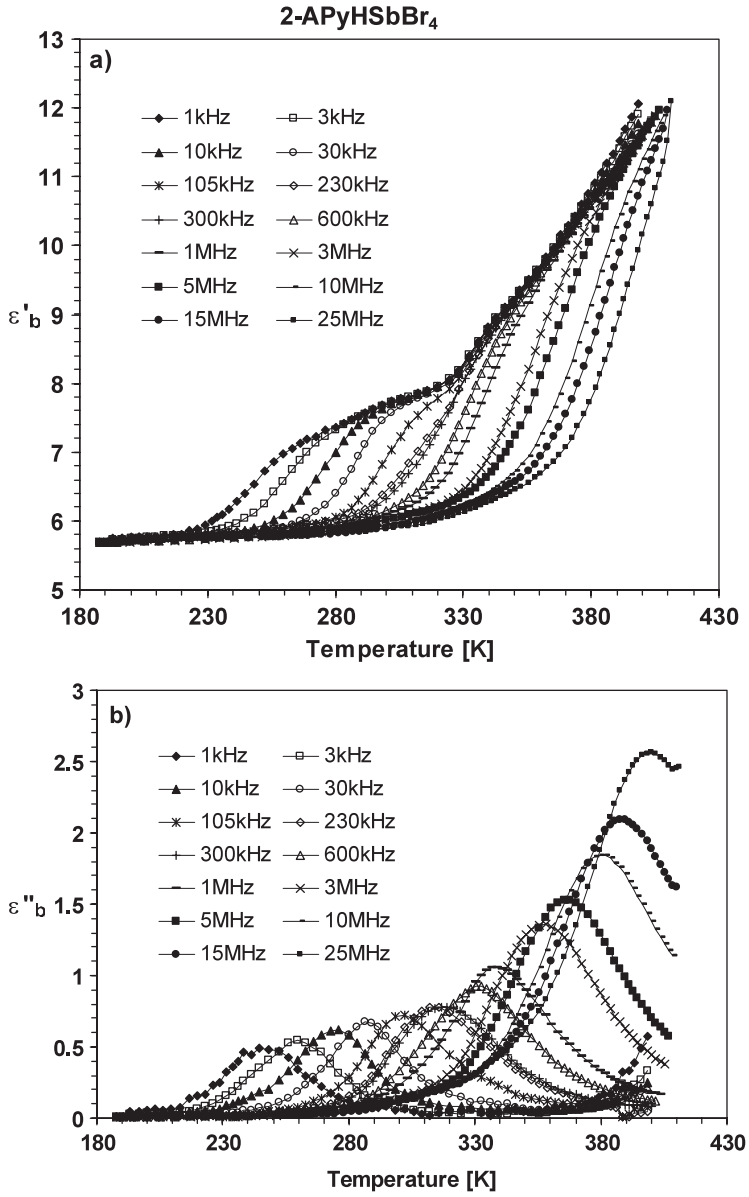

Figure 9. The temperature dependence of (a) the real and (b) the imaginary part of the complex electric permittivity, $\varepsilon_b^* = \varepsilon_b' - \mathrm{i}\varepsilon_b''$, for the 2-APyHSbBr$_4$ samples.

connected with the change of the resultant dipole moment of the unit cell. In our opinion, the most probable motion of the cation is the reorientation about the axis perpendicular to the C_5N plane. The behaviour of ε' versus temperature confirms the discontinuous character of the phase transformation in 2-APyHSbBr$_4$ at 412 K. Moreover, the shape of the dielectric anomaly resembles that for the crystal with 'rotational' phases (plastic crystals), which additionally supports the supposition that we deal with the 'order–disorder' transformation.

This is interesting that below 412 K a clear dielectric absorption and dispersion (see figure 9) at frequencies between 1 kHz and 25 MHz is observed over a wide temperature

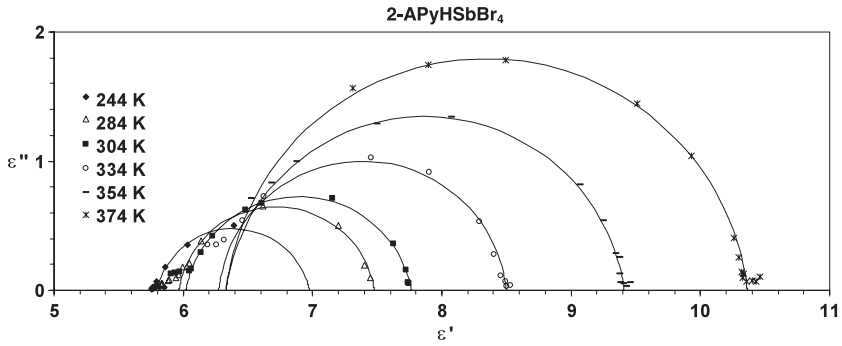

Figure 10. Cole–Cole diagram at selected temperatures for phase II of the 2-APyHSbBr$_4$ samples.

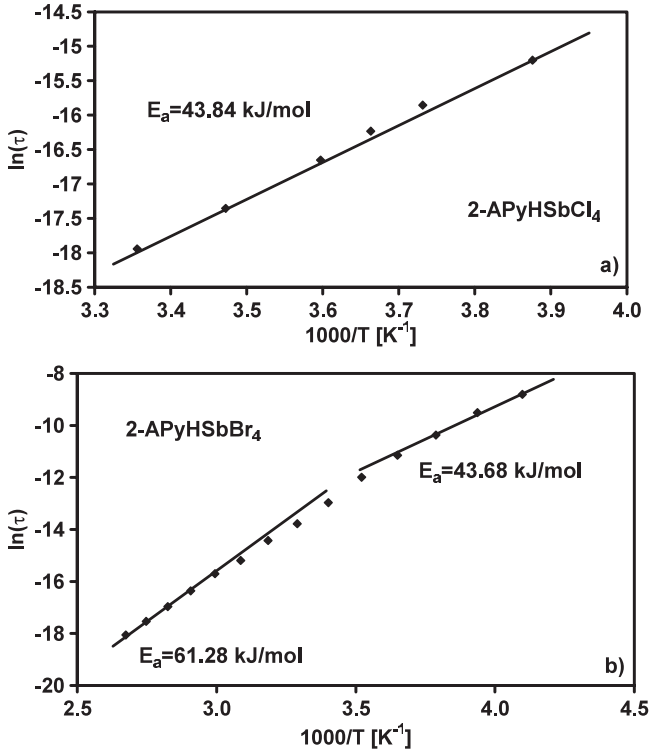

Figure 11. An Arrhenius plot for the dielectric macroscopic relaxation time, $\ln \tau$ versus $1/T$, for 2-APyHSbCl$_4$ and 2-APyHSbBr$_4$.

range, down to 200 K. The parameters of the dielectric relaxation process were estimated at several temperatures using the Cole–Cole relation (1) (see figure 10), similarly to in the case of 2-APyHSbCl$_4$. The parameters of the relaxation process are collected in table 4.

If you carefully analyse the plot of $\varepsilon' = f(T)$ you can see two different regions of dielectric dispersion. One region, between ∼320 and 412 K, is characterized by a larger dielectric increment, $\varepsilon_0 - \varepsilon_\infty$, in comparison to that at temperatures lower than 320 K. This fact is also reflected in a change of the activation energy value, E_a, below and above about 300 K ($1000/T \approx 3.3$, $E_a = 61.28$ and 43.68 kJ mol^{-1}, above and below 320 K, respectively; see figure 11).

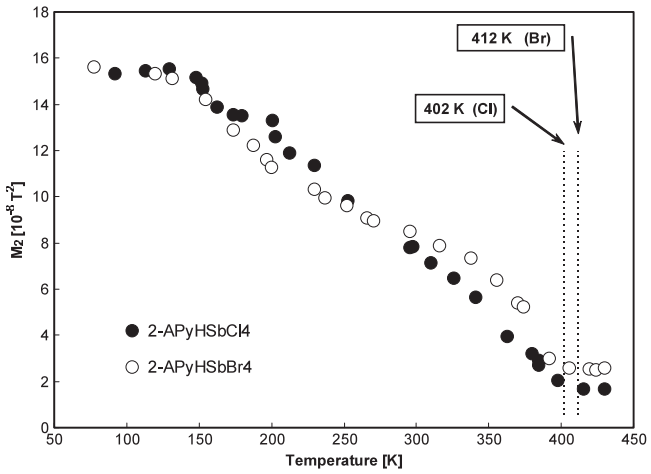

Figure 12. The temperature dependence of the proton second moment, M_2, for 2-APyHSbCl$_4$ and 2-APyHSbBr$_4$.

The cationic motion below ∼320 K is apparently described by a smaller (in comparison to its value above 320 K) change in the dipole moment of the unit cell as a result of the molecular reorientation. It is also characteristic that the parameter of the distribution of relaxation times, α, for 2-APyHSbBr$_4$ is larger below 320 K than above this temperature. This observation may indicate the difference in motional state of the cations above and below about 320 K.

3.5. NMR studies

The temperature changes in the second moment (M_2) of 2-APyHSbCl$_4$ and 2-APyHSbBr$_4$ are shown in figure 12. Over the temperature range in which the ^{1}H NMR signal was studied, the observed line is composed exclusively of a broad component, without any contribution of the narrow component which was e.g. found for the closely related analogue (4-NH$_2$PyH)SbCl$_4$ [22]. Between 77 and 150 K the M_2 value is constant, being about 15.5×10^{-8} T^2 for both analogues; then it starts to decrease monotonically to a value of 2.7×10^{-8} T^2 (2-APyHSbBr$_4$) or to 1.76×10^{-8} T^2 (2-APyHSbCl$_4$) at about 400 K. It should be noted that the M_2 versus temperature curve does not exhibit any anomaly in the vicinity of the phase transition for two analogues. This may suggest that the dynamics of the organic cation changes weakly through the phase transition. The theoretical proton second-moment values were found numerically using our x-ray data for 2-APyHSbCl$_4$ and the Van Vleck formula [23]. Since the x-ray studies do not reveal precise hydrogen atom positions we assumed a normalized geometry of the NH$_2$ group: N–H = 1.00 Å, H–N–H at 120° and C(N)–N = 1.08 Å. Theoretical calculations of the total M_2 (intra-molecular and inter-molecular parts) for a rigid structure of (2-APyHSbBr$_4$) showed that M_2 was equal to 18.4×10^{-8} T^2. The releasing of the motion of the NH$_2$ groups reduces this value to 15.1×10^{-8} T^2, while the onset of a stochastic in-plane reorientation of the 2-APyH cation around a pseudohexagonal C$_6$ symmetry leads to a value of 4.6×10^{-8} T^2. Our experimental results for both crystals clearly show that the last type of motion for both analogues may take place at temperatures above 350 K.

The temperature dependence of the ^{1}H NMR spin–lattice relaxation time (T_1) for 2-APyHSbCl$_4$ (circles) and 2-APyHSbBr$_4$ (squares) is shown in figure 13. Both for

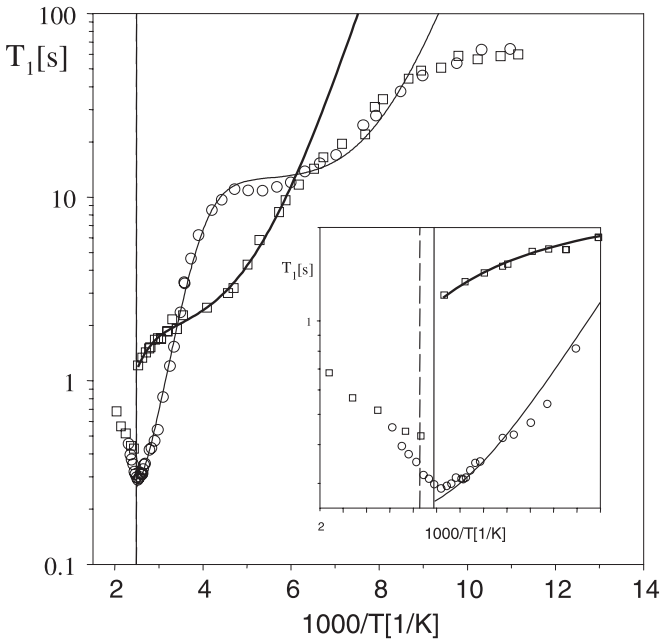

Figure 13. The temperature dependence of the ^{1}H NMR spin–lattice relaxation time, T_1, for 2-APyHSbCl$_4$ (circles) and 2-APyHSbBr$_4$ (squares). The inset shows an enlargement of the area in the main figure in the close vicinity of T_c.

2-APyHSbCl$_4$ and for 2-APyHSbBr$_4$, merely the low temperature side of the minimum of the T_1 versus reciprocal temperature curve is visible. Nevertheless, two different slopes of the curve may be distinguished. In the low temperature phase the value of T_1 for 2-APyHSbCl$_4$ at first minimum is equal to about 10 s and in the case of 2-APyHSbBr$_4$ it is of the order of 2 s.

For 2-APyHSbBr$_4$ the clear jump of T_1 is also observed at the phase transition (412 K). The low temperature part of the T_1 versus reciprocal temperature curve does not exhibit a slope, which could allow us to estimate accurately the dynamical parameters. Above the phase transition the relaxation times are shorter in comparison to those in the low temperature phase and show a tendency to elongate on heating.

The lack of well shaped minima in the spin–lattice relaxation time versus temperature plot prevented us from concluding that we are dealing with an asymmetrical curve originating from the pseudo-C_6 reorientation of the 2-aminopyridinium cation described via a non-equivalent well potential. Thus we decided to adopt the Ito treatment [24] for our results. The main reason for this is the presence of the characteristic double-slope shape of the temperature dependence of the spin–lattice relaxation time, which is very similar to that presented by Ito (for pyridinium salts—$PyAuX_4$, X = Cl, Br) in their paper, where two relaxation mechanisms were discussed. The molecular dynamics for the systems is described by the following expression, in which two contributions were taken into account:

$$\frac{1}{T_1} = \gamma_H^2(\Delta M_2)_{\text{intra}}\left[\frac{3a}{(1+2a)^2}f(\tau_{c1}) + \frac{a}{(1+2a)}f(\tau_{c2})\right] \tag{3}$$

where

$$f(\tau_{ci}) = \frac{\tau_{ci}}{1+\omega_H^2\tau_{ci}^2} + \frac{4\tau_{ci}}{1+4\omega_H^2\tau_{ci}^2}; \tag{4}$$

Table 5. The parameters of the fit obtained for the three-well potential model.

Compound	K (s^{-1})	E_1 (kJ mol^{-1})	E_2 (kJ mol^{-1})	E_3 (kJ mol^{-1})
2-APyHSbCl$_4$	1.66×10^{11}	25.5	19.2	6.3
2-APyHSbBr$_4$	2.3×10^{10}	30.5	23.0	6.3

$(\Delta M_2)_{\text{intra}}$ is the difference between the intra-molecular contribution originating from the M_2 value corresponding to the rigid lattice and that related to the motional state of a molecule at temperature high enough that the six orientations of the 2-aminopyridinium cation can be regarded as equivalent with respect to the pseudo-C_6 axis. The correlation times τ_{c1} and τ_{c2} are defined by $\tau_{c1} = (2W_1 + W_2)^{-1}$ and $\tau_{c2} = (W_2 + 2W_3)^{-1}$, where W_1, W_2 and W_3 are the probability rates of the transition in a three-well potential. The population parameter is given by $a = \exp[(E_{i+1} - E_i)/RT]$, where $i = 1, 2$; E_i are the activation energies, which characterize the three-well potential. The probability rates for the transition of the cation between two different wells are defined by $W_1 = K\exp(-E_1/RT)$, $W_2 = K\exp(-E_2/RT)$ and $W_3 = K\exp(-E_3/RT)$, where K is a jumping frequency factor independent of temperature. The solid curves in figure 13 are the best fit for 2-APyHSbCl$_4$ or for 2-APyHSbBr$_4$. The relaxation constant $C = 1.3 \times 10^9\ s^{-2}$ was found from the fitting procedure for 2-APyHSbCl$_4$ and the same value was assumed for 2-APyHSbBr$_4$ (due to the lack of a fully shaped minimum on the line corresponding to the 2-APyHSbBr$_4$ compound, which made it impossible to directly estimate the relaxation constant). The parameters of the fit obtained, given in table 5, show that for both compounds the following relationship between the estimated activation energies may be drawn up: $E_1 \approx 4/3E_2$ and $E_3 \approx 1/3E_2$. The small value of E_3 suggests the possibility of some kind of libration of the cation in the plane of the pyridinium ring in form of 60° angle jumps between two positions.

4. Discussion

2-APyHSbCl$_4$ and 2-APyHSbBr$_4$ belong to the molecular–ionic crystal group from the halogenoantimonates (III) family. In general the dynamical properties of these crystals are connected with the disorder of the organic cations contributing to the phase transition mechanism. Numerous experimental studies on these salts showed that the symmetry and size of the cations and their ability to form a hydrogen bond system determine the freedom of rotation of molecules in the solid state. In the case of 2-APyHSbCl$_4$ and 2-APyHSbBr$_4$ the cations are able to form hydrogen bonds either with the participation of the NH_2 group or with the N heteroatom of the ring. This is a reason that in the molecular–ionic halogenoantimonates (III) with the 2-APyHMX$_4$ composition the extended network of hydrogen bonding is formed. Even relatively weak hydrogen bonds found in the title compounds (N–H$\cdots$Cl: $\sim$3.38 Å, N–H$\cdots$Br: $\sim$3.48 Å) allow the cations to be fixed in the crystal lattice. This means that in these systems the reorientational disorder of the cations is possible only at high temperatures. Actually the phase transitions in the title crystals have been found above 400 K.

This is a substantially different situation to that observed for the salts containing other substituted pyridinium cations, e.g. 4-aminopyridinium (4-NH_2PyH)SbCl$_4$ [11, 25] or 4-methylpyridinium (4-CH_3PyH)SbCl$_4$ [26], for which the structural phase transitions are observed distinctly below room temperature. These are systems where the hydrogen bondings play a minor role in the stabilization of the cations in the crystal lattice.

The characteristic feature of the salts presented is a great structural similarity. Both salts possess a rigid anionic sublattice and librational disorder of the 2-APyH cations at low temperatures. The structural phase transitions found appear in comparable temperature ranges

(2-APyHSbCl_4—402 K and 2-APyHSbBr_4—412 K). In spite of the facts mentioned above, the essential differences in properties of the crystals are revealed in the type of release of the cationic motions on heating and in the character of the phase transition (the transition close to continuous and the clearly discontinuous one for 2-APyHSbCl_4 and 2-APyHSbBr_4, respectively).

The mechanism of the phase transitions for the 2-APyH salts may be discussed for 2-APyHSbCl_4 and 2-APyHSbBr_4 on the basis of the dielectric dispersion and ^{1}H NMR studies. The first method allows determining the dynamics of dipolar molecules contributing to the electric polarizability of the systems. In our case the anionic sublattice consisting of the polymeric anionic chains ($(SbX_4^-)_\infty$) does not contribute to the dynamic dielectric properties of the crystals since it is rigid. In turn the 2-APyH cations are clearly dipolar units, since 2-APyH is bestowed a significant dipole moment. They are loosely bonded to the halogen atoms by the hydrogen bonds and they are able to perform reorientational motions. The question arises of which kind of the motion of the organic cation we deal with in the crystal lattice. The crystallographic results indicate that the wide-angle librational motions of the cations should be responsible for the dynamical properties at low temperatures of phase II for both crystals.

The dielectric relaxation processes observed in the low temperature phase of 2-APyHSbCl_4 and 2-APyHSbBr_4 are revealed in the frequency range 10^3–10^6 Hz. The relatively long macroscopic relaxation time (10^{-4}–10^{-7} s) as well as the markedly large value of the activation energy (40–60 kJ mol^{-1}) are characteristic of the reorientational motions of bulky organic cationic systems, e.g. *n*-propylammonium or isopropylammonium: [*n*-$C_3H_7NH_3$]$_3$[Sb_2Cl_9]—29 kJ mol^{-1} [20] and [$(CH_3)_2CHNH_3$]$_2$[MX_5]—27–31 kJ mol^{-1} [21]. The significant broad distribution of relaxation times for 2-APyHSbCl_4, $\alpha \approx 0.45$, is an unexpected effect. It is most probably related to the presence of two non-equivalent cations in the structure, which simultaneously contribute to the relaxation process. This is understood as the presence of two dielectric relaxators. Their relaxation time values are very close, which makes it impossible to separate these two dielectric processes. In turn, in 2-APyHSbBr_4 the dielectric relaxation process is almost mono-dispersive. This is consistent with the fact that in the crystal structure of 2-APyHSbBr_4 there is only one type of 2-APyH cation in the unit cell, which corresponds to the one dielectric relaxator found in the relaxation process.

The proton NMR second moment also indicates the dynamical disorder of the dipolar organic cations postulated from the dielectric relaxation investigations. Thus, wide-angle librational motions of cations at temperatures above ∼200–250 K are proposed. Then, above 350 K, even a free C_6'-type rotation of the 2-APyH cations is suggested.

The jump of the ^{1}H NMR relaxation time, T_1, is observed only for the bromine analogue, 2-APyHSbBr_4, which confirms the discontinuous character of the 412 K transition. Such a temperature characteristic of T_1 indicates also the distinct change in the dynamical state of the cations and may be explained in terms of the release of their C_6'-type reorientation above T_c. Moreover, the release of such motion explains the large dielectric increment for this crystal, $\Delta\varepsilon \sim 5$–6 units, at ∼412 K (see figure 8).

In the case of 2-APyHSbCl_4 the evolution from the librational motion of the cations to their free reorientation of the C_6' type follows in a continuous way on heating, which is evidenced by the lack of any anomaly in T_1 around 402 K. This is also consistent with the dielectric response of 2-APyHSbCl_4. The $\varepsilon'_{\text{static}}$ value monotonically increases from ∼11 to 27 units in the temperature range between 310 and 402 K on heating.

In conclusion, it should be emphasized that the changes in the dipolar group dynamics with temperature determine both the dielectric and dynamical properties of phase II in both crystals and give the main contribution to the 'order–disorder' mechanism of the phase transition in 2-APyHSbCl_4 and 2-APyHSbBr_4.

Acknowledgment

This work was supported by the Polish State Committee for Scientific Research (project register 3 T09A 049 26).

References

[1] Jakubas R and Sobczyk L 1990 *Phase Transit.* **20** 163
[2] Varma V, Bhattacharjee R, Vasan H N and Rao C N R 1992 *Spectrochim. Acta* A **48** 1631
[3] Sobczyk L, Jakubas R and Zaleski J 1997 *Pol. J. Chem.* **71** 265 and references cited therein
[4] Jakubas R, Krzewska U, Bator G and Sobczyk L 1988 *Ferroelectrics* **77** 129
[5] Zaleski J and Pietraszko A 1996 *Acta Crystallogr.* B **52** 287
[6] Kawai T, Takao E, Shimanuki S, Iwata M, Miyashita A and Ishibashi Y 1999 *J. Phys. Soc. Japan* **68** 2848
[7] Jakubas R 1989 *Solid State Commun.* **69** 267
[8] Lefebvre J, Carpentier P and Jakubas R 1995 *Acta Crystallogr.* B **51** 167
[9] Jóźków J, Bator G, Jakubas R and Pietraszko A 2001 *J. Chem. Phys.* **114** 7239
[10] Kuok M H, Ng S G, Tan I S, Rang Z I, Iwata M and Ishibasi Y 1998 *Solid State Commun.* **108** 159
[11] Jakubas R, Ciunik Z and Bator G 2003 *Phys. Rev.* B **67** 24103
[12] Czapla Z, Dacko S and Waśkowska A 2003 *J. Phys.: Condens. Matter* **15** 3793
[13] Oxford Diffraction 2001 *CrysAlis 'CCD' and CrysAlis 'RED'* (Wrocław: Oxford Diffraction (Poland)) Sp. z o.o
[14] Sheldrick G M 1997 *SHELXS97* Program for solution of crystal structures, University of Göttingen
[15] Sheldrick G M 1997 *SHELXL97* Program for crystal structure refinement, University of Göttingen
[16] Porter S K and Jacobson R A 1970 *J. Chem. Soc.* A 1356
[17] DeHaven P W and Jacobson R A 1976 *Cryst. Struct. Commun.* **5** 31
[18] Hendrixson T, Horst M A and Jacobson R A 1990 *J. Crystallogr. Spectrosc. Res.* **20** 105
[19] Cole K S and Cole R H J 1941 *Chem. Phys.* **9** 341
[20] Ciąpała P, Zaleski J, Bator G, Jakubas R and Pietraszko A 1996 *J. Phys.: Condens. Matter* **8** 1957
[21] Jakubas R, Bator G, Ciąpała P, Zaleski J, Baran J and Lefebvre J 1995 *J. Phys.: Condens. Matter* **7** 5335
[22] Medycki W, Hołderna-Natkaniec K, Świergiel J and Jakubas R 2003 *Solid State Nucl. Magn. Reson.* **24** 209
[23] Van Vleck J H 1948 *Phys. Rev.* **74** 1168
[24] Ito Y, Asaji T, Ikeda R and Nakamura D 1988 *Ber. Bunsenges. Phys. Chem.* **92** 885
[25] Hashimoto M, Hashimoto S, Terao H, Kuma M, Niki H and Ino H 2002 *Z. Naturf.* a **55** 167
[26] Kulicka B, Jakubas R, Ciunik Z, Bator G, Medycki W, Świergiel J and Baran J 2004 *J. Phys. Chem. Solids* **65** 871